

# PROFILE MONITORS BASED ON RESIDUAL GAS INTERACTION \*

P. Forck, A. Bank, T. Giacomini, A. Peters

Gesellschaft für Schwerionenforschung GSI, Darmstadt, Germany, p.forck@gsi.de

## Abstract

The precise determination of transverse beam profiles at high current hadron accelerators has to be performed non-interceptingly. Two methods will be discussed based on the excitation of the residual gas molecules by the beam particles: First, the beam induced fluorescence (BIF) where light is emitted from the residual gas molecules (in most cases  $N_2$ ) and observed with an image intensified CCD camera. Secondly, by detecting the ionization products in an Ionization Profile Monitor (IPM) where an electric field is applied to accelerate all ionization products toward a spatial resolving Micro-Channel Plate. The signal read-out can either be performed by observing the light from a phosphor screen behind the MCP or electronically by a wire array. Methods to achieve a high spatial resolution and a fast turn-by-turn readout capability are discussed.

## INTRODUCTION

Various methods for the transverse profile determination are used, most of them are based on energy loss of the beam particles in matter or on nuclear reactions at a target material. But for high current hadron beams, non-intercepting methods are preferred to prevent the risk of material melting by the large beam power deposition. The diagnostics must be non-intersecting in order to monitor the undisturbed properties of a beam stored in a synchrotron at any time during the cycle. Even in a pulsed LINAC it might be important to have access to possible time varying processes during the macro-pulse. Two types of non-destructive methods are described here, based on atomic collisions between the beam ions and the residual gas within the vacuum pipe. These methods are: The detection of single photons from excited levels of the residual gas atoms or molecules by **Beam Induced Fluorescence (BIF)** and the direct detection of ionized residual gas ions or electrons at an **Ionization Profile Monitor (IPM)**. In particular IPMs are installed at most hadron synchrotrons and storage rings, but due to the various beam parameters at different laboratories no 'standard realization' is available. The basic features for both methods are discussed and their applicability are compared.

## BEAM INDUCED FLUORESCENCE

In most LINACs and transfer-lines  $N_2$  dominates the residual gas composition. Due to the electronic stopping

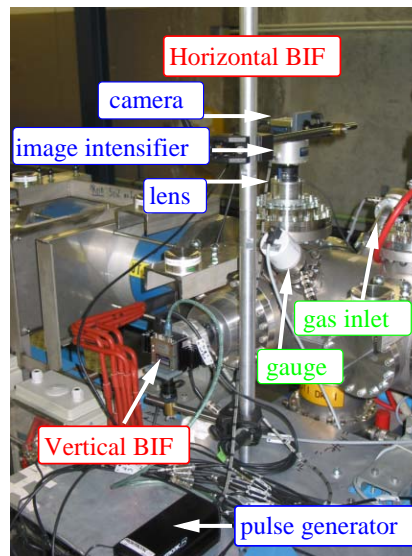


Figure 1: The installation of BIF station at GSI [6].

power the molecules are ionized and with a certain probability left in an excited state. A strong fluorescence in the blue wavelength range  $390 \text{ nm} < \lambda < 470 \text{ nm}$  is generated by a transition band to the  $N_2^+$  electronic ground state ( $B^2\Sigma_u^+(v') \rightarrow X^2\Sigma_g^+(v'') + \gamma$ , for vibrational levels  $v$ ), having a lifetime of about 60 ns [1]. Tests with other gases e.g. Xe were performed, but in this case a lower photon yield in the optical wavelength range was reported [2].

The low amount of photons can be detected and amplified using an image intensifier. This commercially available device consists of a photo cathode to transform the photons into electrons and amplifies them by a spatial resolving MCP electron multiplier. It is followed by a phosphor screen to create again photons, which are finally monitored by a CCD camera. A single primary photon can be amplified to yield  $10^4$  to  $10^7$  detectable photons on the CCD. The photon amplification depends on an adequate choice for the image intensifier components: Various types of photo-cathodes are available offering a different sensitivity with respect to the photon wavelength interval, see e.g. [3]. In general, a photo-cathode sensitive to longer wavelength results in a larger dark current. The photo-electrons can be amplified by a single MCP with typically  $10^3$  electron-multiplication or a double MCP assembly (Chevron configuration) with typically  $10^6$ -fold multiplication. Due to the enlarged distribution of the secondary electrons on several channels at the second MCP, the light spots on the phosphor screen are about a factor 3 larger compared to an single MCP. Depending on the application the required light detection threshold has to be balanced

\* Partly funded by INTAS under Ref. No. 03-54-3931 and by European Union under EU-FP6-CARE-HIPPI

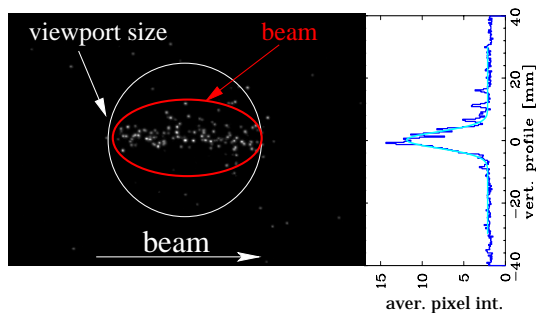


Figure 2: The two dimensional image from the intensifier of a  $\text{Ar}^{10+}$  beam at 4.7 MeV/u and  $I_{beam} = 2.5$  mA recorded during *one* 250  $\mu\text{s}$  long macro-pulse with a vacuum pressure of about  $10^{-5}$  mbar and the projection for the vertical beam profile (right) are shown [6].

with respect to the spatial resolution. Different phosphor screens can be used: Types with fast decay constants of the emitted light of less than 100 ns but lower quantum efficiency (e.g. P47) have to be used if rapid variations have to be monitored. Slower types with typical ms decay times (e.g. P43) offer an increased sensitivity. Instead of using an MCP-phosphor assembly, the BIF-process can also be observed with a segmented photo-multiplier, see e.g. [2, 4].

The hardware set-up, as used for tests at GSI, is displayed in Fig. 1. The BIF-method was pioneered at the Los Alamos proton LINACs [5] for high current dc-beams at MeV energies.

### Example for BIF at a pulsed LINAC

The GSI UNILAC is a pulsed heavy ion LINAC with a macro pulse length of about 100  $\mu\text{s}$  to fill the succeeding synchrotron. The beam profile should be monitored within a single macro pulse; therefore the use of a long integration time for an improved signal-to-noise ratio is impossible. Due to the low amount of emitted photons during typically 200  $\mu\text{s}$  integration time, a large amplification of  $10^6$  is required by a double MCP inside the image intensifier [3]. A P47 phosphor screen with 70 ns decay time is used to monitor fast beam width variations. A raw image is displayed in Fig. 2 together with the vertical profile as yielded from the projection along the beam path [6]. The correspondence of the measured profile to other methods is excellent.

Each of the light spots on the raw image is created by one single photon. Due to the statistical nature of the signal generation, the data quality can be enhanced by data binning or by averaging several images. The resolution of 300  $\mu\text{m}/\text{pixel}$  is sufficient for the displayed parameters. A higher resolution can be reached by varying the distance between the beam pass and the camera and by a proper choice of the optics. This flexible adaption for higher resolution is only limited by the required focal-depth for an accurate mapping. By using a regulated gas valve the pressure could be locally (within 1 m) raised up to  $10^{-4}$  mbar. The pressure bump does not show a measurable influence on the ion beam delivered to the GSI synchrotron. For

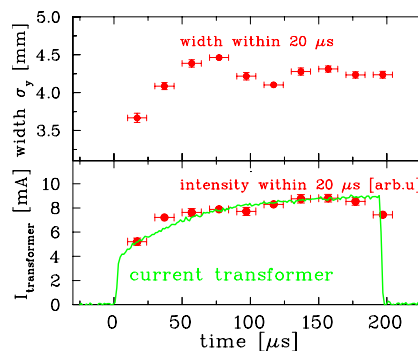


Figure 3: The width variation during a macro-pulse of 8 mA  $\text{Ar}^{10+}$  at 11 MeV/u is shown. The lower graph compares the normalized image intensity with the beam current [6].

some beam settings a relatively large background was seen, caused by neutrons or  $\gamma$  hitting the photo-cathode. Due to the homogeneous distribution it can be subtracted, but a shielding against neutrons might be required for a fail-save application.

An advanced application is the determination of a possible and in most cases unwanted variation of the beam profile during the macro pulse, as shown in Fig. 3. Within a rise time of  $\tau_{rise} = 100$  ns the voltage between the photo-cathode and the MCP can be switched from blocking mode to photo-electron transmission toward the MCP. This can be used to restrict the exposure time during the profile measurement. For the case of Fig. 3 one image of 20  $\mu\text{s}$  exposure time is recorded and these short term measurements are repeated with 10 different trigger delays for consecutive macro-pulses. This time-resolved profile determination is not possible with an intersecting SEM-grid due to the risk of wire melting by the large beam power.

### Example for BIF at Synchrotrons

Careful investigations have been performed at the PS-Booster and the PS at CERN for proton beams [2]. Here the wavelength spectrum and photon yield was measured on a wide scale of beam energies from 50 MeV up to 25 GeV. For a  $\text{N}_2$  pressure bump the wavelength spectrum is comparable to the results obtained for proton collisions at 200

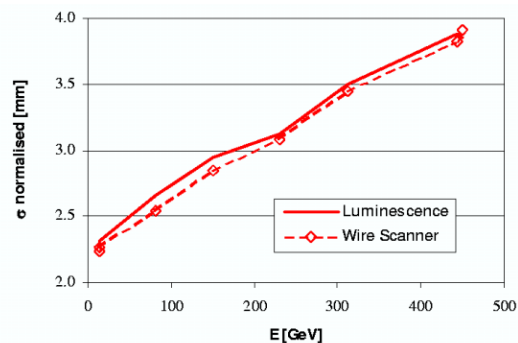


Figure 4: Comparison of the normalized vertical profile width as determined by the BIF-method and a flying wire scanner at CERN-SPS [7].

keV [1]. The lifetime of the excited states was determined using a circulating  $\sim 5$  ns long bunch at 25 GeV energy and observing the decay time using a photo-multiplier. The result of  $\tau = 58.0(3)$  ns coincides with the determination for 100 keV. The absolute photon yield in the optical wavelength range coincide with the calculated electronic stopping power as a function of kinetic energy (Bethe-Bloch formula) and is equivalent to the ion's energy loss of about 3.6 keV in  $N_2$ . Tests with other gases did not result in a larger photon yield.

A BIF monitor was successfully installed at the CERN-SPS [7]. For a pressure bump of  $N_2$  in the order of  $10^{-7}$  mbar profiles within 20 ms integration time, corresponding to about 900 turns, were recorded with sufficient statistical accuracy. A comparison with the standard flying wire scanner method is shown in Fig. 4, proving the applicability of this method also at high energy synchrotrons.

### Example for BIF at ion sources

Behind proton sources, where the protons are only accelerated by the  $\sim 100$  kV potential of the ion source platform these types of measurement are performed in several labs, e.g. [8]. The light yield is large and a long integration time enables careful investigations concerning possible signal broadening processes. A comparison of different gases shows a good correspondence, as displayed in Fig. 5. Taking the different excited levels and lifetimes into account, this result is not evident.

A broadening, in particular at the beam edges was reported [8], therefore the wavelength spectra with varying angles with respect to the beam axis were measured. Due to the angle-dependent Doppler-shift, the fluorescence originating from the residual gas (nearly at rest) and light emitted by the beam particles can be discriminated. The Balmer lines, emitted by the beam protons via recombination  $p+e^- \rightarrow H^* \rightarrow H^0 + \gamma$  or charge-exchange collisions (like  $p + N_2 \rightarrow H^* + N_2^+ \rightarrow H^0 + \gamma + N_2^+$ ) was detected, as well as lines from neutral and charged hydrogen molecules ( $H_2, H_2^+, H_3^+$ ). It can be concluded that the applicability of the BIF method has to be carefully checked to prevent misinterpretation due to the complex processes and large residual gas densities close to an ion source. Prob-

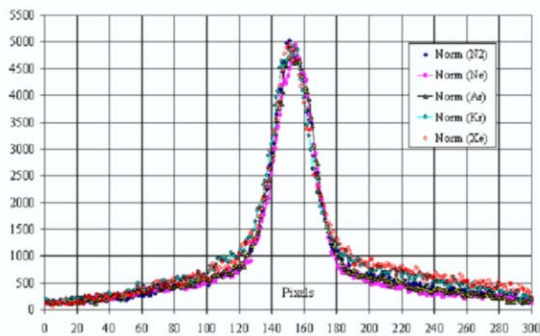


Figure 5: The measured beam profile for different gases determined at the SILHI facility [8].

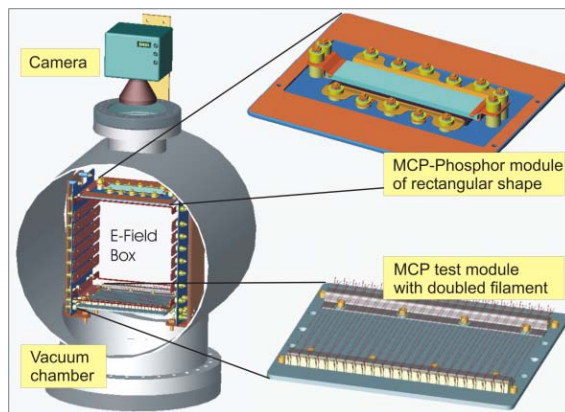


Figure 6: Schematic sketch of an IPM.

bly, this problem does not appear after acceleration by a LINAC due to a single composition of beam ions and the decreasing cross section for electron capture processes at energies above a few 100 keV [9]. But for all cases the residual gas density should be low enough to prevent for second order excitation of the gas molecules via electron excitation like  $N_2 + e^- \rightarrow N_2^* + e^- \rightarrow N_2 + \gamma + e^-$  [1]. As a rough criterion the mean free path of electrons should be much larger than the beam size, which is only valid for a pressure below  $p < 10^{-3}$  mbar.

## IONIZATION PROFILE MONITOR

In most synchrotrons and storage rings the transverse profile of the circulating beam is monitored by detecting the ionization products from the collision of the ions with the residual gas (mainly  $H_2$ ). Inside the vacuum tube biased electrodes produce an electric field of typically 10 to 50 V/mm to accelerate the secondary electrons or ions toward an MCP, as shown schematically in Fig. 6. In the detection volume below the MCP a large electric field homogeneity is required (typically better than 1 %) to guide the residual gas ions on a straight trajectory toward the MCP resulting in an undistorted beam image. Most IPMs are equipped with a double MCP to yield a  $\sim 10^6$ -fold electron multiplication for a single particle detection scheme. As stated in the BIF description the spatial resolution is about a factor 3 worse compared to a single MCP. Two different anode readout technologies for the amplified signal are commonly in use:

- *Phosphor screen:* The electrons create light spots on a phosphor screen behind the MCP, which are monitored by a CCD camera, as shown schematically in Fig. 6. A high spatial resolution can be achieved with this readout method, only limited by the  $\sim 50 \mu m$  granularity of the double MCP channel size. Therefore this method is preferred in cooler rings. A typical time resolution is in the order of 10 ms, given by the frame rate of the CCD camera. For a turn-by-turn readout on a  $\mu s$  time scale the CCD camera is too slow. A multi-anode photomultiplier [10] or a photo-diode

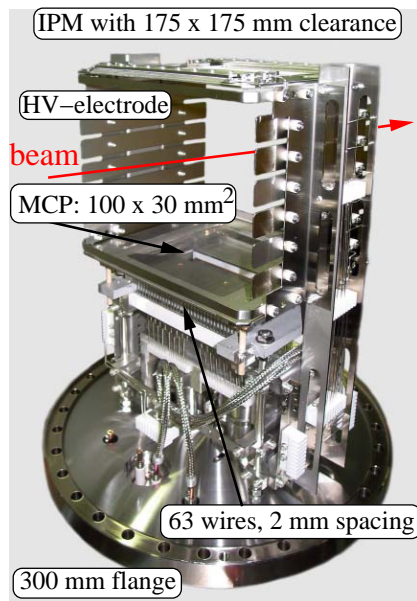


Figure 7: Photo of the IPM at the GSI synchrotron [15].

array [11, 12] has to be installed as a second readout system.

- **Wire array:** An array of wires can be mounted behind the MCP to collect the current of amplified electrons; a technical realization is shown in Fig. 7. The spatial resolution down to 0.5 mm, as given by the distance of the anode wires, is less than for the phosphor screen readout. But it is possible to get a time resolution of  $\sim 10$  ns using sensitive broadband rf-amplifiers [13]. When monitoring a bunched beam, a carefully designed shielding-pass for the beam image current has to be foreseen to prevent for distortions by a capacitive signal pick-up.

The surface-coating inside the MCP-channels shows non-recoverable amplification decrease after reaching a certain irradiation level as caused by the electron bombardment at the exit side of the MCP. To visualize this local non-uniformity of the MCP-amplification a test device has to be foreseen. One can install a filament-array on the HV-electrode opposite to the MCP, which is heated in regular, typically monthly time intervals to emit thermal electrons. Recently, an Electron Generator Plate (EGP) has been used to achieve a homogeneous electron emission [14]. Alternatively, the MCP can be illuminated by a UV-lamp [15]. In case of amplification degradation the MCP has to be exchanged or a software correction of the sensitivity has to be applied.

Depending on the voltage polarity for the electric field generation IPMs can be operated to detect residual ions or electrons. For low current beam applications residual ion detection is normally chosen and no magnetic field is required. Due to the scattering kinematics a negligible momentum is transferred to the residual gas ions and they are accelerated only on straight trajectories by the external electric field. For beam currents as normally stored in

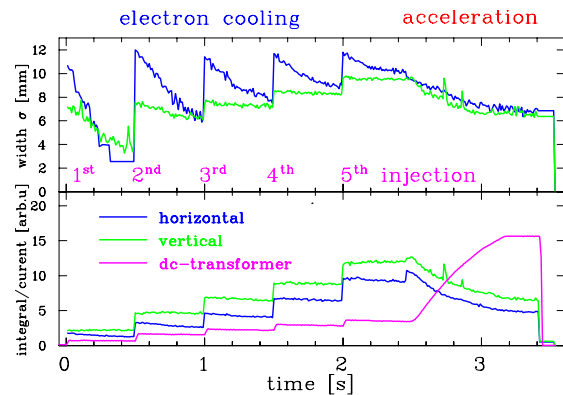


Figure 8: The process of beam stacking by electron cooling of a 11.4 MeV/u  $U^{73+}$  beam during 5 injections followed by an acceleration to 400 MeV/u at the GSI synchrotron is monitored. The horizontal and vertical beam width  $\sigma$  during the 3.4 s long cycle is shown on top and the integral of the individual profiles as well as the dc-transformer on bottom. Each 10 ms a profile is recorded [15].

high power synchrotrons, the space-charge field  $\mathbf{E}_{SC}$  of the beam is comparable to the IPM electric field. To overcome the influence of  $\mathbf{E}_{SC}$  an electron detection scheme is used, where the electrons are guided towards the MCP by a magnetic field of typically  $B = 100$  mT. This value is chosen so that the cyclotron radius  $r_c$  along a field line is comparable to the resolution of the MCP. The cyclotron radius  $r_c = m_e v_{\perp} / eB$  is mostly determined by the initial electron velocity  $v_{\perp}$  perpendicular to the  $B$ -field after the atomic collision. It can be estimated that 90 % of these electrons are emitted with kinetic energies below 50 eV, resulting in  $r_c < 100 \mu\text{m}$ . A well-defined  $B$ -field uniformity is required along the full path of the secondary electrons from the interaction point to the MCP (up to 100 mm) to yield an undistorted image of the beam. To estimate the possible distortion due to the beam space-charge (via  $\mathbf{E}_{SC} \times \mathbf{B}$ -drift) and the residual  $B$ -field non-uniformity, numerical calculations of the electron trajectories are required, see e.g. [12]. Different magnet designs have been realized, using either electro-magnets [10] or permanent magnets [13, 16].

Operating an IPM with an electron detection scheme the residual gas ions hit the electric field electrode opposite to the MCP. Special care has to be taken to prevent surface-emitted electrons reaching the MCP, either by a special electrode-coating by e.g. NEG-material or by installing a negatively biased grid in front of the electrode.

One important application is the alignment of the electron- or stochastic cooling process [15]. As displayed in Fig. 8, electron cooling is applied to stack the beam via iterative injections. Other applications are the monitoring of the beam behavior during emittance blow-up due to intra beam scattering, necessary crossing of tune resonances or a horizontal-vertical coupling due to skew quadrupoles. For these processes significant changes of the transverse profile are slow compared to the revolution period, therefore a time resolution of ms is sufficient and the transverse profile can be averaged over many turns. The high spatial resolu-

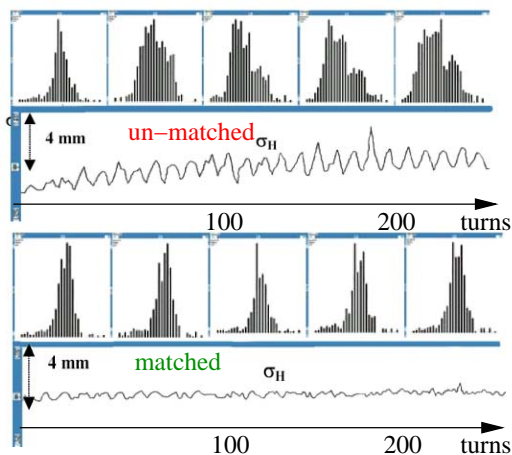


Figure 9: Horizontal beam evolution on a turn-by-turn basis and the associated rms beam width for an un-matched and matched case [10].

tion by a phosphor screen anode and a CCD camera is well suited for this application.

But also fast processes must be monitored on a turn-by-turn basis [10, 13, 16]. An example is the control of the injection matching into a synchrotron as displayed in Fig. 9. If the orientation of the injected transverse emittance (as given by the transfer beam line setting) does not correspond to the values at the synchrotron injection point, damped beam width oscillations occur leading to an emittance blow-up of the stored beam. A matched setting of the transfer line lattice, controlled by the non-destructive IPM, is required to achieve high brilliant beams. For turn-by-turn measurements during the accelerating cycle special HV-switching techniques for the MCP have to be applied to overcome the regular count rate limitation (typically  $10^6$  counts per second in the stationary case) and enabling a measurement with sufficient statistics of at least 100 events within one turn (i.e. down to  $1 \mu\text{s}$ ), see e.g. [16].

At transfer lines the residual density is orders of magnitude larger. In particular, behind a LINAC the ionization rate can be large enough to measure this ionization directly with sensitive current-to-voltage amplifiers. An MCP is not required for this application reducing the mechanical efforts drastically.

## COMPARISON BETWEEN BIF AND IPM

The BIF-method detects photons and no mechanical installation inside the vacuum tube is required. Commercial image intensifiers are available, and commercial data acquisition and evaluation systems can be used, reducing the amount of human resources during the development phase. The spatial resolution as given by the optical magnification of the lens system is easily changeable and can be matched to the application. A resolution of  $100 \mu\text{m}$  can be reached and is sufficient for most application at a hadron accelerator. At transfer-lines the residual gas density is relatively large and therefore the amount of detectable photons is higher than at synchrotrons. But compared to the detec-

tion of ionization products the photon yield is reduced by at least one order of magnitude because particular levels have to be excited for the emission in the optical range. Only those photons, which are emitted toward the camera can be detected, resulting in a solid angle of only  $\Delta\Omega \sim 10^{-4}$ . A further reduction is required by a limited iris setting of the optics to ensure a sufficient focal-depth. Background contribution due to neutrons or  $\gamma$ s hitting the photo-cathode might occur for some beam settings. The lack of radiation hardness for the CCD camera electronics might be a disadvantage, because for an effective light collection the distance to the beam can not be very large.

The IPM detects all charged residual gas particles due to the applied electric field, but the complex and expensive installation of the electric field generation and the MCP detector inside the vacuum tube is required. For intense beams a magnetic field must guide the residual gas electrons toward the MCP. Its design might be a challenge due to the uniformity requirement and the anomalous large clearance of up to 400 mm. The spatial resolution of  $\sim 100 \mu\text{m}$  as given by the MCP channel size is sufficient for most applications at a hadron synchrotron. Resolution limits are presently investigated by the comparison to a wire scanners [17]. At synchrotrons the vacuum pressure has to be much lower compared to transfer-lines. Therefore the  $\sim 10^5$  times larger signal strength for the IPM (comparing 'single particle detection' in both cases) is required to enable sufficient time resolution. In particular, IPMs offers the possibility to perform turn-by-turn profile measurements on a  $\mu\text{s}$  time scale, which has not been demonstrated with BIF so far.

## REFERENCES

- [1] R.H. Hughes et al., *Phys. Rev.* **123**, 2084 (1961), L.W. Dotchin et al., *J. Chem. Phys.* **59**, 3960 (1973).
- [2] M.A. Plum et al., *Nucl. Instrum. Meth A* **492**, p. 42 (2002).
- [3] see e.g. [www.proxitronic.de](http://www.proxitronic.de).
- [4] J. Dietrich et al., *Proc. ICFA-Hadron Beams 05, Bensheim* (2004).
- [5] D.P. Sandoval et al., *Proc. Beam Instrum. Workshop, Santa Fe, AIP Conf. Proc.* **319**, p. 273 (1993).
- [6] P. Forck, A. Bank, *Proc. EPAC 02, Paris*, p. 1885 (2002) and A. Bank, P. Forck, *Proc. DIPAC 03, Mainz*, p. 137 (2003).
- [7] G. Burtin et al., *Proc. EPAC 2000, Vienna*, p. 256 (2000).
- [8] P. Ausset et al., *Proc. EPAC02, Paris*, p. 1840 (2002).
- [9] R.H. Hughes et al., *Phys. Rev. A* **1**, 1424 (1970), R.H. Hughes et al., *Phys. Rev.* **164**, 166 (1967).
- [10] G. Ferioli et al., *Proc. DIPAC01, Grenoble*, p. 201 (2001), G. Ferioli et al., *Proc. DIPAC03, Mainz*, p. 116 (2003), C. Fischer et al., *Proc. Beam Instrum. Workshop, Knoxville, AIP Conf. Proc.* **732**, p. 133 (2004).
- [11] S. Barabin et al., *Proc. EPAC04, Lucerne*, p. 2721 (2004).
- [12] D. Liakin et al., *Proc. DIPAC05, Lyon* (2005).
- [13] P. Cameron et al., *Proc. PAC99, New York*, p. 2114 (1999), R. Connolly et al., *Proc. PAC01, Chicago*, p. 1297 (2001).
- [14] H. Refsum et al., *Proc. DIPAC05, Lyon* (2005).
- [15] T. Giacomini et al., *Proc. Beam Instrum. Workshop, Knoxville, AIP Conf. Proc.* **732**, p. 286 (2004), T. Giacomini et al., *Proc. DIPAC05, Lyon* (2005).
- [16] J.R. Zagel et al., *Proc. PAC01, Chicago*, p. 1303 (2001), J.R. Zagel et al., *Proc. PAC99, New York*, p. 2164 (1999).
- [17] C. Fischer et al., *Proc. EPAC04, Lucerne*, p. 2478 (2004).